Available online at www.sciencedirect.com
SCIENCE DIRECT®
International Journal of Heat and Mass Transfer 49 (2006) 2762–2770
International Journal of HEAT and MASS TRANSFER
www.elsevier.com/locate/ijhmt

Thermal analysis on metal-foam filled heat exchangers. Part II: Tube heat exchangers

C.Y. Zhao [a,b,*], W. Lu [b], S.A. Tassou [b]

[a] State Key Laboratory of Multiphase Flow and Heat Transfer, School of Energy and Power Engineering, Xi'an Jiaotong University, Shaanxi 710049, PR China
[b] Department of Mechanical Engineering, School of Engineering and Design, Brunel University, Uxbridge, Middlesex UB8 3PH, UK

Received 8 September 2005
Available online 20 March 2006

Abstract

The forced convection heat transfer characteristics in high porosity open-cell metal-foam filled tube heat exchangers are analysed in this paper. The Brinkman-extended Darcy momentum model and two-equation heat transfer model for porous media are employed for the analysis of the heat transfer performance. The morphological effects of metal foams on overall heat transfer are examined. The optimal foam-area ratio for a metal-foam filled counter-flow tube-in-tube heat exchanger is predicted. The study shows that the thermal performance of a metal-foam heat exchanger can be superior to that of conventional finned tube heat exchangers.

1. Introduction

Recently, the use of high porosity metal foams have spread to include applications, such as aircraft wing structures for the aerospace industry, catalytic surfaces for chemical reactions, core structures for high strength panels, and containment matrices and burn rate enhancers for solid propellants [1,2]. Due to the high surface-area density and strong mixing capability for the fluid, open-cell metal foams are now regarded as one of the most promising materials for the manufacture of efficient compact heat exchangers.

In principle, high porosity metal foams with open cells can be treated as porous media. For metal-foam filled tube heat exchangers the Brinkman-extended Darcy model [3] and two-equation non-equilibrium heat transfer model [4] can be employed as the momentum and energy equations, respectively. The two-equation non-equilibrium heat transfer model treats the solid ligaments of metal foams and the fluid separately.

When the difference in the thermal conductivities of the fluid and solid is significant, as is the case in this study, the temperature difference between local fluid and solid phases cannot be neglected, Calmidi and Mahajan [5]. In these situations the two-equation non-equilibrium heat transfer model should be employed for the analysis of the heat transfer performance in metal-foam filled tube heat exchangers [6].

Even though from the heat transfer point of view metal foams can be considered as a type of porous media, they have very distinctive features such as high porosities and a unique open-cell morphology that need special treatment. A number of investigations on the thermal transport of high porosity open-cell metal foams have been carried out during the last fifteen years. Calmidi and Mahajan [5] and Zhao et al. [7] conducted experimental and numerical studies for air-cooled forced convection in metal-foam filled plate channels. Heat transfer measurements on compressed aluminium-foam heat exchanger arrays have been performed by Boomsma et al. [8] to evaluate their performance in industrial applications. Aluminium foams for duct heat

* Corresponding author. Address: Department of Mechanical Engineering, School of Engineering and Design, Brunel University, Uxbridge, Middlesex UB8 3PH, UK. Tel.: +86 298 266 8036/+44 1895 266697; fax: +44 1895 266697/256392.
E-mail addresses: cyzhao@mail.xjtu.edu.cn, chang-ying.zaho@brunel.ac.uk (C.Y. Zhao).

0017-9310/$ - see front matter © 2006 Elsevier Ltd. All rights reserved.
doi:10.1016/j.ijheatmasstransfer.2005.12.014

Nomenclature

$\tilde{a}$	surface area density (m^{-1})
A	surface area (m^2)
Da	Darcy number, K/R^2
D_H	hydraulic diameter (m)
h	heat-transfer coefficient (W/m^2K)
h_{sf}	interfacial heat-transfer coefficient of metal foams (W/m^2K)
H	depth of the fins or grooves (m)
k	thermal conductivity (W/m K)
k_e	effective thermal conductivity
K	permeability (m^2)
Nu	Nusselt number, hD_H/k_f
Nu_{sf}	local Nusselt number, $h_{sf}d_p/k_f$
Pr	Prandtl number, $c_p\mu_f/k$
p	pressure (Pa)
P	dimensionless pressure
q_w	heat flux (W/m^2)
Q	heat (J)
R	inner radius of the inner tube (m)
R_1	outer radius of the inner tube (m)
R_2	inner radius of the outer tube (m)
Re	Reynolds number, $2uR/\upsilon$
S	pitch of spiral groove (m)
t	thickness (m)
T	temperature (K)
u	velocity along z-direction (m/s)
u_m	mean velocity along z-direction (m/s)
U	dimensionless velocity along z-direction, u/u_m
U_i	overall heat-transfer coefficient based on the inside area of the inner tube (W/m^2K)

Greek symbols

ε	porosity
θ	dimensionless temperature, $\frac{T-T_w}{q_wR/k_{se}}$
$\sum$	sum
ρ	density (kg/m^3)
μ_f	dynamic viscosity (kg/m s)
υ	kinematic viscosity (m^2/s)
ψ	dimensionless radial coordinate, r/R_1

Subscripts

s	solid
f	fluid
w	wall
i	inside of inner tube
o	outside of inner tube

exchangers have also been investigated by Tadrist et al. [9]. Both studies showed that aluminium foams can enhance the heat transfer capability of the heat exchangers. In addition, Boomsma et al. [8] studied the required coolant pumping power against thermal resistance and demonstrated that foams can have significantly higher efficiencies over several conventional heat exchangers.

The heat transfer performance of metal-foam filled pipe was discussed in Part I of this paper. In this second part, the heat transfer performance of metal-foam filled tube-in-tube heat exchanger is analysed. The effects of different parameters (such as pore size, porosity, geometrical size, etc.) on the heat transfer and fluid flow performance of metal-foam tube heat exchangers is discussed. Furthermore, the overall performance of a metal-foam filled tube heat exchanger is compared with that of a conventional finned tube heat exchanger.

2. Physical problem

The problem under consideration in this paper is the analysis of the thermal performance of a counter-flow tube-in-tube heat exchanger as shown in Fig. 1. The heat exchanger comprises of two concentric pipes forming an inner section and an outer annular section, both filled with metal foams. Fluid flows axially through both sections in a counter-flow arrangement. The outer pipe is assumed to be perfectly insulated so there is no heat transfer between the pipe's outer surface area and the surroundings. The heat

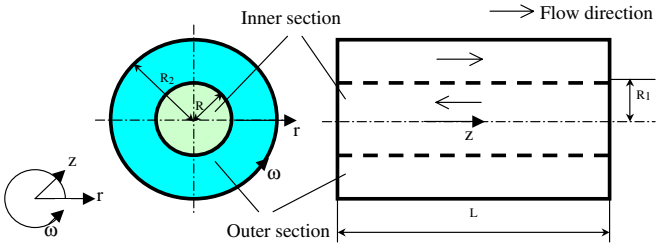

Fig. 1. A schematic diagram of a tube-in-tube heat exchanger filled with metal foam.

flux through the wall of the inner pipe is assumed to be constant so the thermal boundary conditions of the inner surface of the outer section can be assumed to constant heat flux. The solution for the inner pipe was presented in Part I of this paper. The solution for the outer pipe is presented in the following sections.

3. Mathematical formulation and analytical solution

3.1. Mathematical formulation and normalisation

As mentioned earlier, the Brinkman extended Darcy momentum model [3] and the two-equation non-equilibrium heat transfer model proposed by Calmidi and Mahajan [5] are employed in the analysis for both the fluid and solid. For fully developed flow, these equations can be simplified to one-dimensional differential equations as follows:

• Momentum equation

$$0 = -\frac{\mathrm{d}p}{\mathrm{d}z} + \frac{\mu_\mathrm{f}}{\varepsilon}\left(\frac{\partial^2 u}{\partial r} + \frac{1}{r}\frac{\partial u}{\partial r}\right) - \frac{\mu_\mathrm{f}}{K}u \tag{1}$$

• Energy balance equations for the solid and fluid

$$0 = k_\mathrm{se}\left(\frac{\partial^2 T_\mathrm{s}}{\partial r^2} + \frac{1}{r}\frac{\partial T_\mathrm{s}}{\partial r}\right) - h_\mathrm{sf}\tilde{a}(T_\mathrm{s} - T_\mathrm{f}) \tag{2}$$

$$\varepsilon\rho_\mathrm{f}C_\mathrm{f}u\frac{\mathrm{d}T_\mathrm{f}}{\mathrm{d}z} = k_\mathrm{fe}\cdot\left(\frac{\partial^2 T_\mathrm{f}}{\partial r^2} + \frac{1}{r}\frac{\partial T_\mathrm{f}}{\partial r}\right) + h_\mathrm{sf}\tilde{a}(T_\mathrm{s} - T_\mathrm{f}) \tag{3}$$

For the inner section (as shown in Fig. 1), the boundary conditions are

$$\text{When } r = R, \quad u = 0, \quad T_\mathrm{s} = T_\mathrm{f} = T_\mathrm{w} \tag{4}$$

$$\text{When } r = 0, \quad \frac{\partial u}{\partial r} = \frac{\partial T_\mathrm{f}}{\partial r} = \frac{\partial T_\mathrm{s}}{\partial r} = 0 \tag{5}$$

For the outer section, when constant heat flux is imposed on the interface between the inner pipe wall and metal-foam and the outer boundary is insulated, the boundary conditions are

$$\text{When } r = R_1, \quad u = 0, \quad T_\mathrm{s} = T_\mathrm{f} = T_\mathrm{w} \tag{6}$$

$$\text{When } r = R_2, \quad u = 0, \quad \frac{\partial T_\mathrm{f}}{\partial r} = \frac{\partial T_\mathrm{s}}{\partial r} = 0 \tag{7}$$

The details of solving the equations for the inner section are described in the companion paper I. The solution of the equations for the outer section is given below, to non-dimensionalise the equations the following variables are employed:

$$\begin{aligned} &Da = K/R_1^2, \quad \psi = r/R_1, \quad P = \frac{K}{\mu_\mathrm{f}u}\frac{\mathrm{d}p}{\mathrm{d}z}, \\ &\theta = \frac{T - T_\mathrm{w}}{q_\mathrm{w}R_1/k_\mathrm{se}}, \quad \theta_\mathrm{s} = \frac{\langle T\rangle_\mathrm{s} - \langle T\rangle_\mathrm{w}}{q_\mathrm{w}R_1/k_\mathrm{se}}, \\ &\theta_\mathrm{f} = \frac{\langle T\rangle_\mathrm{f} - \langle T\rangle_\mathrm{w}}{q_\mathrm{w}R_1/k_\mathrm{se}}, \quad D = h_\mathrm{sf}\tilde{a}R_1^2/k_\mathrm{se}, \\ &C = \frac{k_\mathrm{fe}}{k_\mathrm{se}}, \quad U = \frac{u}{u_\mathrm{m}} \end{aligned} \tag{8}$$

where u and u_m are the local and mean velocities along the axial direction, respectively.

The equations for outer section can be normalised as

$$U = -P + \frac{Da}{\varepsilon}\left(\frac{\partial^2 U_z}{\partial\psi} + \frac{1}{\psi}\frac{\partial U_z}{\partial\psi}\right) \tag{9}$$

$$0 = \frac{\partial^2\theta_\mathrm{s}}{\partial\psi^2} + \frac{1}{\psi}\frac{\partial\theta_\mathrm{s}}{\partial\psi} - D(\theta_\mathrm{s} - \theta_\mathrm{f}) \tag{10}$$

$$2U\left(\frac{1}{\left(\frac{R_2}{R_1}\right) - 1}\right) = C\cdot\left(\frac{\partial^2\theta_\mathrm{f}}{\partial\psi^2} + \frac{1}{\psi}\frac{\partial\theta_\mathrm{f}}{\partial\psi}\right) + D(\theta_\mathrm{s} - \theta_\mathrm{f}) \tag{11}$$

$$\psi = 1, \quad U = \theta_\mathrm{s} = \theta_\mathrm{f} = 0 \tag{12}$$

$$\psi = R_2/R_1, \quad U = 0, \quad \frac{\partial\theta_\mathrm{s}}{\partial\psi} = \frac{\partial\theta_\mathrm{f}}{\partial\psi} = 0 \tag{13}$$

3.2. Analytical solution of the equations

The above equations can be treated as equations in the form of $\frac{\partial^2 Y}{\partial z^2} + \frac{1}{z}\frac{\partial Y}{\partial z} - Y = 0$ and $\frac{\partial^2 Y}{\partial z^2} + \frac{1}{z}\frac{\partial Y}{\partial z} = C$. The latter is easy to solve. The standard solutions of the former, $J_0(z)$ and $Y_0(z)$ are given in Appendix A. Based on this, Eqs. (9)–(11) can be analytically solved subject to boundary conditions (12) and (13).

• The dimensionless velocity distribution

The velocity distribution can be obtained by solving momentum equation (9), as

$$U = P\left(N_1\cdot J_0\left(\sqrt{\frac{\varepsilon}{Da}}\psi\right) + N_2\cdot Y_0\left(\sqrt{\frac{\varepsilon}{Da}}\psi\right)\right) - P \tag{14}$$

since $\frac{1}{A}\int_A U\,\mathrm{d}A = 1$, solving for P the following is obtained:

$$P = \frac{(R_2/R_1)^2 - 1}{2\sqrt{\frac{Da}{\varepsilon}}\left(N_1\left(\frac{R_2}{R_1}\cdot J_1\left(\sqrt{\frac{\varepsilon}{Da}}\frac{R_2}{R_1}\right) - J_1\left(\sqrt{\frac{\varepsilon}{Da}}\right)\right) + N_2\left(\frac{R_2}{R_1}Y_1\left(\sqrt{\frac{\varepsilon}{Da}}\frac{R_2}{R_1}\right) - Y_1\left(\sqrt{\frac{\varepsilon}{Da}}\right)\right)\right) - \left(\frac{R_2}{R_1}\right)^2 + 1} \tag{15}$$

• The dimensionless temperature distribution

After the velocity distribution is determined, the temperature profile can be obtained by solving Eqs. (10) and (11).

$$\begin{aligned} \theta_\mathrm{s} = {} & \frac{2P}{\left(\frac{R_2}{R_1}\right)^2 - 1}\left(-\frac{1}{4}\psi^2 + N_3\ln\psi + N_4 + N_1\frac{Da}{\varepsilon}J_0\left(\sqrt{\frac{\varepsilon}{Da}}\psi\right)\right. \\ & \left. + N_2\frac{Da}{\varepsilon}Y_0\left(\sqrt{\frac{\varepsilon}{Da}}\psi\right)\right) - C\theta_\mathrm{f} \end{aligned} \tag{16}$$

$$\begin{aligned} \theta_\mathrm{f} = {} & \frac{2P}{C+1}\left(\frac{1}{\left(\frac{R_2}{R_1}\right)^2 - 1}\left(-\frac{1}{4}\psi^2 + N_3\ln\psi + N_4 + \left(A + \frac{Da}{\varepsilon}\right)\right.\right. \\ & \times\left(N_1J_0\left(\sqrt{\frac{\varepsilon}{Da}}\psi\right) + N_2Y_0\left(\sqrt{\frac{\varepsilon}{Da}}\psi\right)\right) \\ & \left.\left. - \left(N_5J_0\left(\sqrt{\frac{(C+1)D}{C}}\psi\right) + N_6Y_0\left(\sqrt{\frac{(C+1)D}{C}}\psi\right)\right) + B - A\right)\right) \end{aligned} \tag{17}$$

where

$$A = \frac{1}{\left(C\cdot\frac{\varepsilon}{Da} - (C+1)\cdot D\right)}$$

and

$$B = \frac{C}{(C+1)\cdot D\cdot\left(C\cdot\frac{\varepsilon}{Da} - (C+1)\cdot D\right)}$$

$$N_1=\frac{Y_0\left(\sqrt{\frac{\varepsilon}{Da}}\right)-Y_0\left(\sqrt{\frac{\varepsilon}{Da}}R_2\right)}{J_0\left(\sqrt{\frac{\varepsilon}{Da}}R_2\right)\cdot Y_0\left(\sqrt{\frac{\varepsilon}{Da}}\right)-Y_0\left(\sqrt{\frac{\varepsilon}{Da}}R_2\right)\cdot J_0\left(\sqrt{\frac{\varepsilon}{Da}}\right)}$$

$$N_2=\frac{J_0\left(\sqrt{\frac{\varepsilon}{Da}}\right)-J_0\left(\sqrt{\frac{\varepsilon}{Da}}R_2\right)}{Y_0\left(\sqrt{\frac{\varepsilon}{Da}}R_2\right)\cdot J_0\left(\sqrt{\frac{\varepsilon}{Da}}\right)-J_0\left(\sqrt{\frac{\varepsilon}{Da}}R_2\right)\cdot Y_0\left(\sqrt{\frac{\varepsilon}{Da}}\right)}$$

$$N_3=\frac{R_2}{R_1}\left(\frac{1}{2}\frac{R_2}{R_1}-\frac{Da}{\varepsilon}\left(N_1J_1\left(\sqrt{\frac{\varepsilon}{Da}}R_2\right)+N_2Y_1\left(\sqrt{\frac{\varepsilon}{Da}}R_2\right)\right)\right)$$

$$N_4=\frac{1}{4}-\frac{Da}{\varepsilon}\left(N_1J_0\left(\sqrt{\frac{\varepsilon}{Da}}\right)+N_2Y_0\left(\sqrt{\frac{\varepsilon}{Da}}\right)\right)$$

$$N_5=\frac{B\cdot Y_1\left(\sqrt{\frac{(C+1)D}{C}}R_2\right)-N_7\cdot Y_0\left(\sqrt{\frac{(C+1)D}{C}}\right)}{J_0\left(\sqrt{\frac{(C+1)D}{C}}\right)\cdot Y_1\left(\sqrt{\frac{(C+1)D}{C}}R_2\right)-J_1\left(\sqrt{\frac{(C+1)D}{C}}R_2\right)\cdot Y_0\left(\sqrt{\frac{(C+1)D}{C}}\right)}$$

$$N_6=\frac{B\cdot J_0\left(\sqrt{\frac{(C+1)D}{C}}\right)-N_7\cdot J_1\left(\sqrt{\frac{(C+1)D}{C}}R_2\right)}{J_0\left(\sqrt{\frac{(C+1)D}{C}}\right)\cdot Y_1\left(\sqrt{\frac{(C+1)D}{C}}R_2\right)-J_1\left(\sqrt{\frac{(C+1)D}{C}}R_2\right)\cdot Y_0\left(\sqrt{\frac{(C+1)D}{C}}\right)}$$

$$N_7=\sqrt{\frac{\varepsilon}{Da}\frac{C}{(C+1)D}}\cdot A\cdot\left(N_1J_1\left(\sqrt{\frac{\varepsilon}{Da}}R_2\right)+N_2Y_1\left(\sqrt{\frac{\varepsilon}{Da}}R_2\right)\right)$$

• Overall Nusselt number

For the inner surface of the outer section, the overall heat transfer coefficient $\bar{h}_o$ is

$$\bar{h_o}=\frac{q_w}{T_w-T_{f,bo}}=-\frac{k_{se}}{\theta_{f,bo}\cdot R_1} \tag{18}$$

The Nusselt number then becomes

$$\overline{Nu_o}=\frac{\bar{h_o}}{k_f}D_H=-\frac{k_{se}}{k_f\theta_{f,bo}}\frac{D_H}{R_1} \tag{19}$$

where $D_H=2(R_2-R_1)$ and $\theta_{f,bo}$ is the dimensionless bulk-mean fluid temperature averaged over the cross-section of the outer channel. Then,

$$\theta_{f,bo}=\frac{T_{f,b}-T_w}{q_wR_1/k_{se}}=\frac{\int_0^{2\pi}\int_1^{\frac{R_2}{R_1}}U\theta_f\psi\,d\psi\,d\vartheta}{\int_0^{2\pi}\int_1^{\frac{R_2}{R_1}}U\psi\,d\psi\,d\vartheta}=2\int_1^{\frac{R_2}{R_1}}U\theta_f\psi\,d\psi \tag{20}$$

The solutions for the inner section obtained in the companion paper (Part I), are given below:

• The velocity solution

$$U=P\frac{J_0\left(\sqrt{\frac{\varepsilon}{Da}}\psi\right)}{J_0\left(\sqrt{\frac{\varepsilon}{Da}}\right)}-P \tag{21}$$

• The solid and fluid temperature solutions

$$\theta_s=2P\left(-\frac{1}{4}\psi^2+\frac{\frac{Da}{\varepsilon}}{J_0\left(\sqrt{\frac{\varepsilon}{Da}}\right)}J_0\left(\sqrt{\frac{\varepsilon}{Da}}\psi\right)+\frac{1}{4}-\frac{Da}{\varepsilon}\right)-C\theta_f \tag{22}$$

$$\theta_f=\frac{2P}{C+1}\left(-\frac{1}{4}\psi^2+\frac{\frac{Da}{\varepsilon}}{J_0\left(\sqrt{\frac{\varepsilon}{Da}}\right)}J_0\left(\sqrt{\frac{\varepsilon}{Da}}\psi\right)+\frac{1}{4}-\frac{Da}{\varepsilon}-B\cdot\frac{1}{J_0\left(\sqrt{\frac{(C+1)D}{C}}\right)}\cdot J_0\left(\sqrt{\frac{(C+1)D}{C}}\psi\right)+A\cdot\frac{1}{J_0\left(\sqrt{\frac{\varepsilon}{Da}}\right)}J_0\left(\sqrt{\frac{\varepsilon}{Da}}\psi\right)+\frac{1}{(C+1)\cdot D}\right) \tag{23}$$

• Overall heat transfer coefficient

$$h_i=\frac{q_w}{T_{wi}-T_{f,bi}}=-\frac{k_{se}}{\theta_{f,bi}R} \tag{24}$$

In the solution for the inner section, R is used as the length scale.

4. Results and discussion

4.1. Dimensionless velocity and temperature distributions

Figs. 2 and 3 show the predicted dimensionless velocity and temperature distributions, respectively, in the inner and outer tubes of the metal-foam filled tube heat exchanger. The curves in the centre part of the diagrams represent the distributions in the inner tube, and the curves at two ends represent the distributions in the outer tube. As can be seen from Fig. 2, the shape of the dimensionless velocity distribution in the outer tube is similar to that in the inner tube, with the velocity increasing from zero at the boundary (tube wall) to its maximum value in the centre of the passage.

In the equation of the dimensionless temperature, $\theta=\frac{T-T_w}{q_wR_1/k_{se}}$, q_w is positive when the fluid absorbs heat from the wall and negative when the fluid transfers heat to the wall. As expected, Fig. 3 shows that the temperatures of the fluid and solid are the same on the boundary wall. In the inner tube, the fluid temperature reduces from maximum in the centre to minimum on the pipe wall. The temperature variation in the foam, although of similar trend, is much more gradual than the temperature variation in the fluid. Unlike the dimensionless temperature distribution

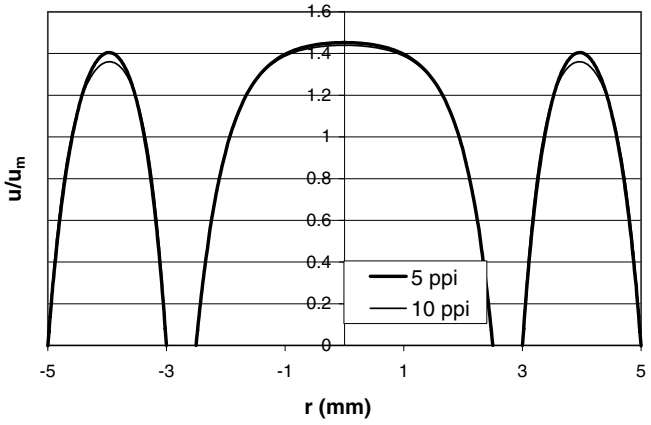

Fig. 2. Dimensionless velocity distribution in a metal-foam tube-in-tube heat exchanger.

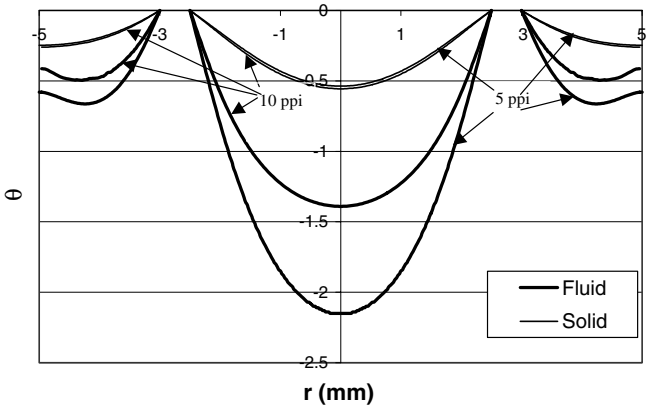

Fig. 3. Dimensionless temperature distribution in a metal-foam tube-in-tube heat exchanger.

in the inner tube, the dimensionless solid (foam) temperature in the outer tube decreases from the inner wall to reach minimum value on insulated wall. The dimensionless fluid temperature first decreases from the inner wall to a minimum at the centre of the passage and then increases slightly towards the outer wall. Fig. 2 also shows that increasing the pore density improves the velocity distribution and reduces the temperature difference between the solid and fluid (Fig. 3).

4.2. Heat transfer performance in metal-foam filled compact heat exchanger

4.2.1. Heat transfer in outer annular channel

To apply this analytical solution to the metal-foam filled tube heat exchanger, the fluid flow and heat transfer through the metal-foam filled annular channel (outer tube) is analysed (the heat transfer performance of the inner tube was discussed in the companion paper, Part I). Figs. 4 and 5 show the heat transfer performance for air flow in the outer tube filled with different metal foams. Similar to the results for the inner tube (Part I), Fig. 4 shows that decreasing either the porosity or pore size leads to an increase in the heat transfer performance. It is also shown in Fig. 5 that increasing the solid thermal conductivity or fluid velocity can enhance heat transfer performance. The effect of fluid velocity is greater for higher thermal conductivity foams.

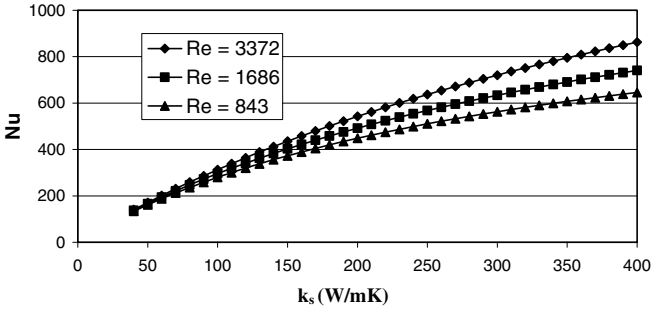

Fig. 5. Variation of Nusselt number in the outer tube with solid thermal conductivity (k_s) and Reynolds number.

4.2.2. Overall heat transfer coefficient for metal-foam heat exchangers

The overall heat transfer in a metal-foam filled tube-in-tube heat exchanger can be expressed as

$$Q = U_i A_i (T_A - T_B) \tag{25}$$

where $U_i = \frac{1}{\frac{1}{h_i}+\frac{R\ln(R_1/R)}{k_s}+\frac{R}{R_1 h_o}}$ [10], $A_i = 2\pi RL$, T_A and T_B are the fluid temperatures, and h_i and h_o are the inside and outside convection heat-transfer coefficients for, respectively. To analyze the effect of the flow cross-sectional area ratio $(\pi R^2/(\pi R_2^2 - \pi R_1^2))$ on the overall heat transfer coefficient, the radius of the outer tube (R_2) was set at 10 mm and the wall thickness of the inner tube ($R_1 - R$) at 0.5 mm. The flow cross-sectional area ratio would therefore vary only with the radius of the inner tube (R). The results are shown in Fig. 6. It can be seen that as the inner tube diameter increases, the cross-sectional area of the inner tube increases and the area of outer channel decreases. This causes an increase in the inside heat transfer coefficient (h_i) and a decrease in the outside heat-transfer coefficient (h_o). As a consequence, the overall heat-transfer coefficient for the heat exchanger (U_i) first increases with increasing h_i to a maximum value at $R = 0.004$ m, and then gradually decreases.

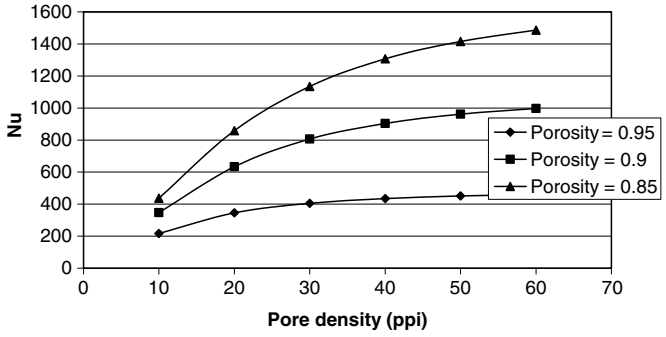

Fig. 4. Variation of Nusselt number with pore density in the outer tube filled with copper foam.

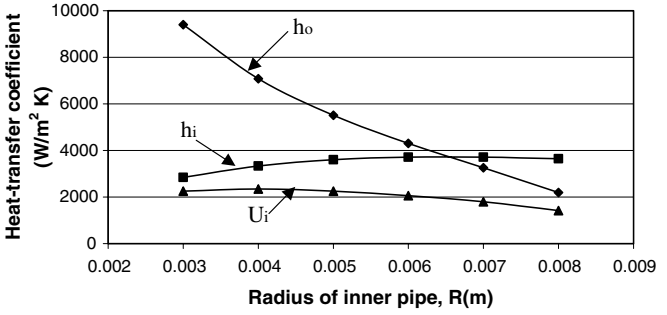

Fig. 6. Relationship between the heat transfer coefficients h_i, h_o and U_i (air velocity = 10 m/s).

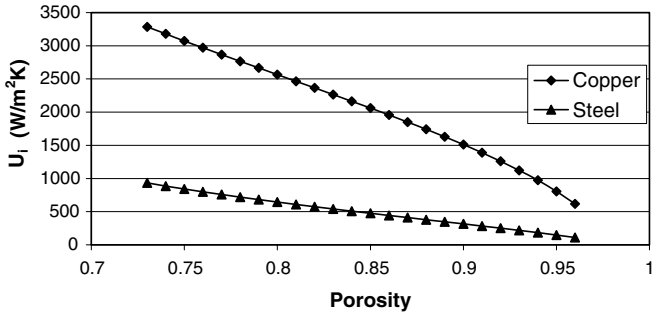

Fig. 7. Variation of overall heat-transfer coefficient of heat exchanger with metal-foam porosity.

Fig. 7 shows the effect of porosity on the overall heat transfer coefficient of the heat exchanger for air velocity through the tubes of 10 m/s. It can be seen that as the porosity increases the overall heat transfer coefficient reduces. Fig. 7 also shows that the overall heat transfer coefficient increases with increase of thermal conductivity, copper exhibits a higher overall heat transfer coefficient than steel, but this increase diminishes as porosity approaches unity. The effect of pore density and flow velocity on the performance of the heat exchanger is shown in Fig. 8. It can be seen that for a constant porosity of 0.9, increasing either the flow velocity or the pore density will lead to an increase in the overall heat transfer coefficient.

4.2.3. Parametric analysis of heat exchanger

From Eq. (25), the overall heat transfer in the heat exchanger can be quantified as $Q = U_i A_i (T_A - T_B) = U_i A_i \Delta T$. If q represents heat transfer per unit length i.e. $q = Q/L$, then $q = U_i 2R\Delta T$ and the heat-transfer capacity of the heat exchanger per unit length becomes $q/\Delta T = U_i 2R$.

Figs. 9 and 10 show the effect of the diameter of the inner tube on the overall heat exchanger thermal performance for air velocity of 10 m/s on both sides. It can be seen that the heat-transfer capacity of the metal-foam filled heat exchanger examined reached maximum at $R = 0.65$ which represents a foam area ratio close to 1.0. It can also be seen that the heat transfer performance of a plain tube

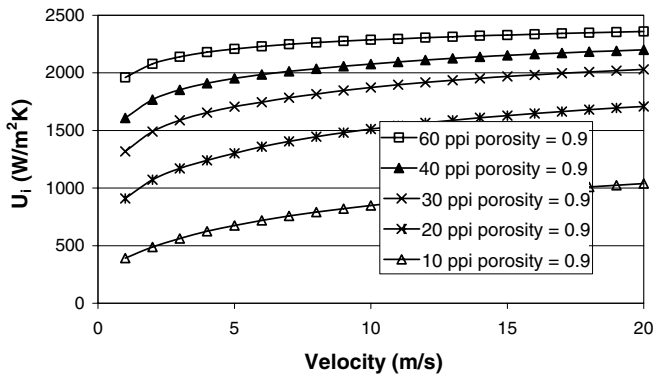

Fig. 8. Variation of overall heat-transfer coefficient of heat exchanger with fluid velocity.

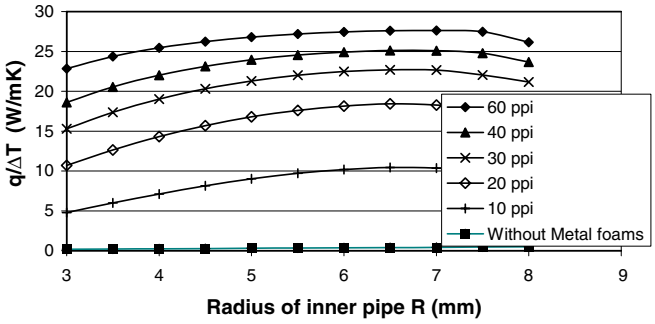

Fig. 9. Variation of heat-transfer capability with the diameter of inner pipe at selected pore densities (porosity = 0.9).

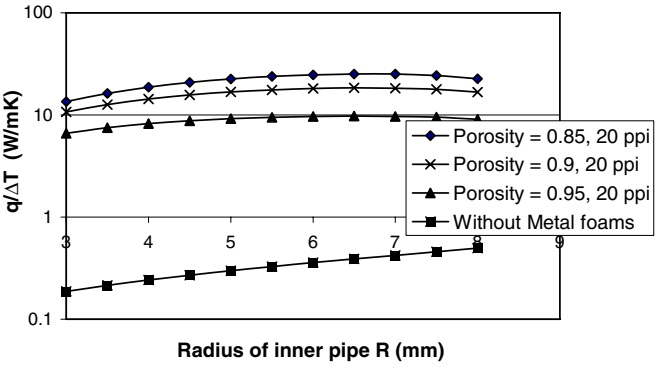

Fig. 10. Variation of heat-transfer capability with the diameter of inner pipe at selected porosities.

heat exchanger is much lower than that of a foam filled heat exchanger and for a foam heat exchanger increasing the pore density leads to an increase in heat transfer performance. Increasing the porosity will cause a reduction in heat transfer performance (Fig. 10).

Fig. 11 shows the influence of the pore density on the optimal inner tube diameter for maximum heat transfer. It can be seen that, with the pore density of the outer tube constant at 20 ppi, increasing the inner tube pore density from 10 ppi to 60 ppi, reduces the optimum inner tube radius from $R = 7.5$ mm to $R = 5$ mm. It can therefore be concluded that the optimum inner tube diameter or flow cross-sectional area ratio varies with the relative pore densities of the metal foams filled on both sides of heat exchanger.

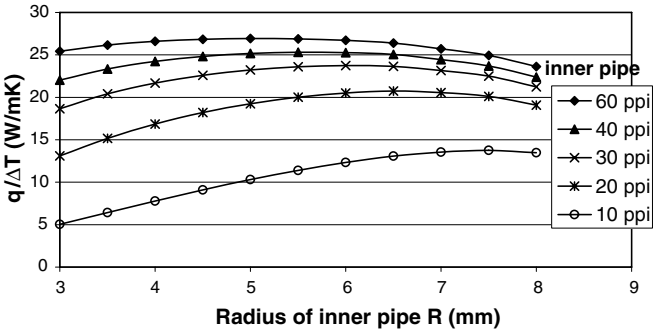

Fig. 11. Variation of the heat-transfer capability with the diameter of inner pipe (porosity = 0.9).

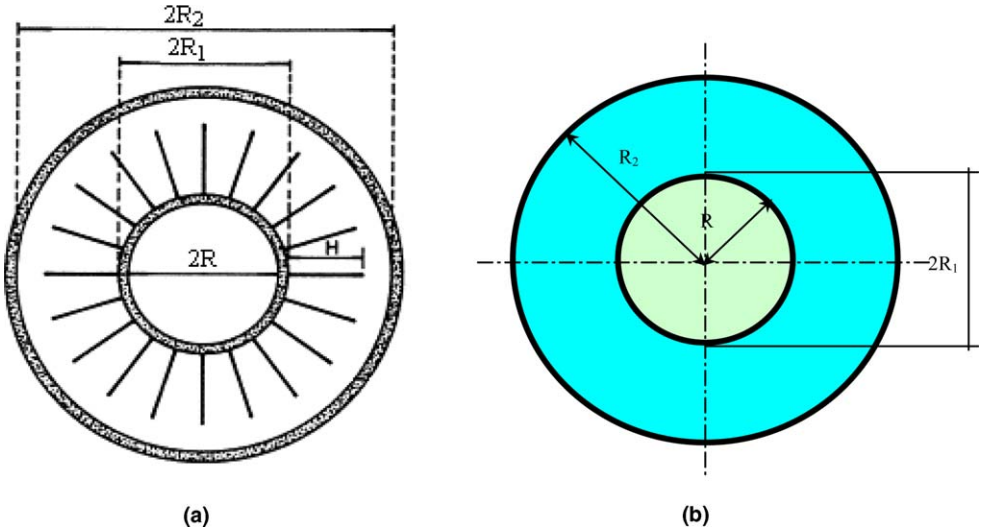

Fig. 12. Geometry of conventional finned tube heat exchanger ($R = 6$ mm, $R_1 = 6.5$ mm, $R_2 = 10$ mm). (a) The heat exchanger with inner grooved tube (spiral grooves: $s = 0.1$ mm, $H = 1$ mm) and fins (longitudinal fins: 20 fins, $H = 2.5$ mm, $t = 0.075$ mm), (b) metal-foam filled heat exchanger.

4.2.4. Comparison with conventional finned tube heat exchangers

Fig. 12 shows the configuration of a conventional finned tube heat exchanger (a) and a metal-foam filled tube-in-tube heat exchanger (b). For the conventional heat exchanger an inner grooved tube is assumed with fins on its external surface to improve heat transfer. For comparison purposes the two heat exchangers are made of copper and air is used as the working fluid on both sides. To widen the range of comparison, both spiral and longitudinal fins of and different fin densities were considered.

To calculate the heat transfer rate of the conventional compact heat exchanger, the following empirical correlations were employed:

For smooth tubes [10]:

$$h_i = \frac{k}{d_i} 0.023 Re_d^{0.8} Pr^{0.3} \tag{26}$$

For spiral groove tubes [11]:

$$h_i = \frac{k}{d_i} 0.363 Re_d^{0.6} Pr^{0.3} (H/d_i)^{0.103} (S/d_i)^{-0.29} \tag{27}$$

The fin efficiency is determined from [10]

$$\eta = \frac{\tanh(mH)}{mH} = \frac{\tanh\left(\sqrt{2h_o/(kt)}H\right)}{\sqrt{2h_o/(kt)}} \tag{28}$$

where H is the depth of the fins or grooves, S is the pitch of the spiral grooves and, t, is the fin thickness.

Figs. 13 and 14 show comparisons between the metal-foam filled annular channel and the finned channels. Longitudinal fins were assumed for Fig. 13, and spiral fins for Fig. 14. Both charts show that the use of metal foams can significantly improve the heat transfer performance due to the enlarged surface area density and strong mixing of fluid flow in metal foams. For the same area density the performance of the foam filled annular tube is approximately

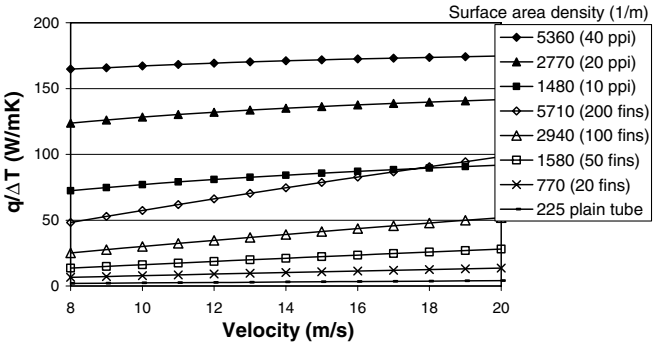

Fig. 13. The effect of velocity on heat transfer performance: metal foams ($\varepsilon = 0.9$) versus longitudinal fins (fin depth = 2.5 mm).

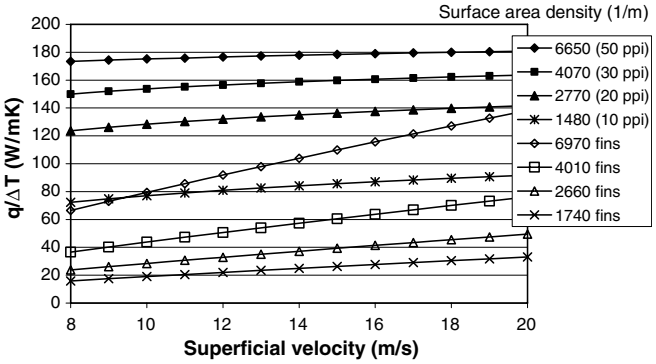

Fig. 14. The effect of velocity on heat transfer performance: metal foams ($\varepsilon = 0.9$) versus spiral fins.

three times higher than the performance of the longitudinally finned tube. Using spiral instead of longitudinal fins improves the performance of the conventional heat exchanger (Fig. 14) but this is still much inferior to the performance of the metal-foam filled annular channel.

Fig. 15 shows a comparison between conventional and metal-foam filled (both core and annular sections)

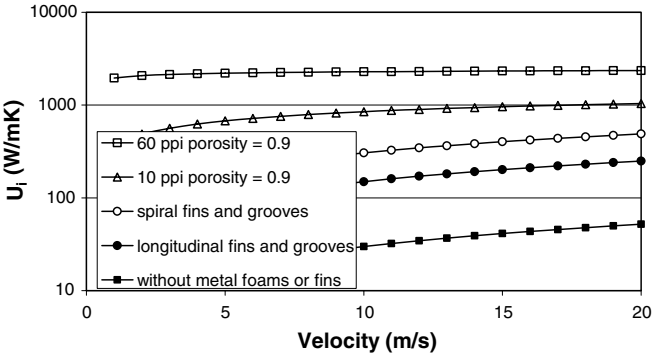

Fig. 15. Comparison between different kinds of heat exchangers.

tube-in-tube heat exchangers. It can be seen that the overall heat transfer coefficient of the metal-foam filled heat exchanger is significantly higher than that of conventional finned tube heat exchangers. For example, the overall heat transfer coefficient of a 10 ppi copper-foam filled heat exchanger is shown to be more than double that of a finned tube heat exchanger (spiral fins 5000 fins/m, $H = 1$ mm, $t = 0.075$ mm and inner tube grooves $S = 0.1$ mm, $H = 1$ mm). Therefore, it is clear that the use of metal foams can greatly enhance the heat transfer, and metal foams have significant potential in the manufacture of compact heat exchangers.

5. Conclusion

In this work, the heat transfer performance of a metal-foam filled tube heat exchanger has been analysed by using the Brinkman-extended Darcy momentum model and the two-equation heat transfer model for porous media. Analytical solutions for temperature and velocity distributions have been obtained for both the inner and outer tubes of a tube-in-tube heat exchanger. It is shown that the heat transfer capacity of the metal-foam filled tube heat exchanger increases with either the increase of pore density (ppi) or the decrease of porosity. The use of metal foams can significantly enhance the heat transfer performance of tube-in-tube heat exchangers compared to that of conventional finned tube heat exchangers due to the high surface area density and strong flow mixing. The results also showed that the heat transfer performance of metal-foam filled tube-in-tube heat exchangers is a function of the ratio of the flow cross-sectional area and relative pore densities of the metal foams filled on both sides of heat exchanger.

Acknowledgements

This work is supported by National Natural Science Foundation of China (No. 50576069), National Basic Research Programme of China (No. 2006CB601203), the UK Engineering and Physical Sciences Research Council (EPSRC grant number: GR/T24364/01), and the Program for New Century Excellent Talents in University (NCET-04-0944), and Brief Award of Brunel University (WAE-DPA301). Financial support by the NSFC Fund for Creative Research Groups (No. 50521604). The authors also wish to thank the assistance of Mr. Ian Stirling, Porvair Plc., for providing test samples.

Appendix A. General solutions of the partial differential equation

For the differential equation of form of

$$z^2 \cdot \frac{\partial^2 Y}{\partial z} + z \cdot p(z) \cdot \frac{\partial Y}{\partial z} + q(z) \cdot Y = 0 \tag{A.1}$$

which is one of the classical functions of mathematical physics [12]. One solution of this equation is: $f(z) = z^{\mu}\sum_{n=0}^{\infty} c_n z^n$. Assuming $p(z) = 1$ and $q(z) = -z^2$, dividing both sides by z^2 and simplifying, Eq. (A.1) takes the form

$$\frac{\partial^2 Y}{\partial z} + \frac{1}{z}\frac{\partial Y}{\partial z} - Y = 0 \tag{A.2}$$

which should be solved in this paper.

Based on the solution of (A.1) the solution of (A.2) is

$$J_0(z) = \sum_{n=0}^{\infty} \frac{1}{(n+v)!n!}\left(\frac{1}{2}z\right)^{2n} \tag{A.3}$$

A second solution of Eq. (A.1) is

$$f(z) = C \cdot J_0(z)\ln(z) + z^{\mu_2}\sum_{n=0}^{\infty} d_n(z) \cdot z^n$$

Applying this to Eq. (A.2) we get

$$Y_0(z) = J_0(z)\ln\left(\frac{1}{2}z\right) + \sum_{n=0}^{\infty} \frac{F_n}{(n+1)!(n+1)!(n+1)}\left(\frac{1}{2}z\right)^{2n+2} \tag{A.4}$$

where $F_n = \frac{n+1}{n}F_{n-1} - 1$ and $F_0 = -1$.

Therefore, the $J_0(z)$ and $Y_0(z)$ are two solutions for Eq. (A.2).

For $J_1(z) = J_0'(z)$, and $Y_1(z) = Y_0'(z)$, $J_1(z)$ and $Y_1(z)$ can be determined as

$$J_1(z) = \left(\frac{1}{2}z\right)\sum_{n=0}^{\infty} \frac{1}{(n+v)!n!}\left(\frac{1}{2}z\right)^{2n} \tag{A.5}$$

$$Y_1(z) = J_1(z)\ln\left(\frac{1}{2}z\right) + \frac{1}{2}\sum_{n=0}^{\infty} \frac{1}{n!n!}\left(\frac{1}{2}z\right)^{2n-1} + \frac{1}{2}\sum_{n=0}^{\infty} \frac{F_n}{(n+1)!(n+1)!}\left(\frac{1}{2}z\right)^{2n} \tag{A.6}$$

Accordingly, the form of the solutions, $(z \cdot J_1(z))' = z \cdot J_0(z)$ and $(z \cdot Y_1(z))' = z \cdot Y_0(z)$ can be obtained.

References

[1] T.J. Lu, H.A. Stone, M.F. Ashby, Heat transfer in open-celled metal foams, Acta Mater. 46 (1998) 3619–3635.

[2] A. Bhattacharya, V.V. Calmidi, R.L. Mahajan, Thermophysical properties of high porosity metal foams, Int. J. Heat Mass Transfer 45 (2002) 1017–1031.

[3] K. Vafai, C.L. Tien, Boundary and inertia effects on flow and heat transfer in porous media, Int. J. Heat Mass Transfer 24 (1981) 195–203.
[4] A. Bejan, Convection Heat Transfer, second ed., Wiley, New York, 1995.
[5] V.V. Calmidi, R.L. Mahajan, Forced convection in high porosity metal foams, J. Heat Transfer 122 (2000) 557–565.
[6] C.Y. Zhao, T. Kim, T.J. Lu, H.P. Hodson, Thermal transport phenomena in Porvair Metal foams and sintered beds, Ph.D. Report, University of Cambridge, 2001.
[7] C.Y. Zhao, T. Kim, T.J. Lu, H.P. Hodson, Thermal transport in high porosity cellular metal foams, J. Thermophys. Heat Transfer 18 (3) (2004) 309–317.
[8] K. Boomsma, D. Poulikakos, F. Zwick, Metal foams as compact high performance heat exchangers, Mech. Mater. 35 (2003) 1161–1176.
[9] L. Tadrist, M. Miscevic, O. Rahli, F. Topin, About the use of fibrous materials in compact heat exchangers, Exp. Therm. Fluid Sci. 28 (2004) 193–199.
[10] J.P. Holman, Heat Transfer, seventh ed., McGraw-Hill, London, 1992.
[11] X.S. Wang, R.Z. Wang, J.Y. Wu, Experimental investigation of a new-style double-tube heat exchanger for heating crude oil using solar hot water, Appl. Therm. Eng. 25 (2005) 1753–1763.
[12] N.M. Temme, Special Functions: An Introduction to the Classical Functions of Mathematical Physics, Wiley, New York, 1996.